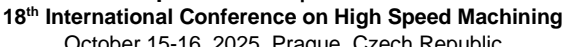


MM Science Journal | www.mmscience.eu

ISSN 1803-1269 (Print) | ISSN 1805-0476 (On-line)

Special Issue | HSM 2025



October 15-16, 2025, Prague, Czech Republic DOI: 10.17973/MMSJ.2025_11_2025132



HSM2025-44964

MATERIAL REMOVAL MECHANISM OF CONTINUOUS FIBER REINFORCED METAL MATRIX COMPOSITES DURING HIGH SPEED GRINDING WITH SINGLE CBN GRAIN

Biao Zhao1 and Wenfeng Ding1*

¹College of Mechanical and Electrical Engineering, Nanjing University of Aeronautics and Astronautics, Nanjing 210016, China

*Corresponding author. Email: dingwf2000@vip.163.com (W.F. Ding)

Abstract

Continuous fiber reinforced metal matrix composites (CFMMCs) show great potential in aerospace industry due to their high specific strength, excellent high-temperature resistance, improved fatigue performance, and lightweight properties. Grinding plays a pivotal role in machining difficult-to-cut materials, including ceramic composites and metal matrix composites. However, the process often results in severe surface defects, such as matrix smearing, fiber fragmentation, and delamination, due to the high toughness of the metal matrix, the high hardness and brittleness of reinforcing fibers, and the inherent anisotropy and heterogeneity of composites. This study employs high-speed grinding (HSG) with singlegrain abrasives to process SiC_f/TC17 composites, aiming to improve the removal of matrix and fibers. Furthermore, this study investigates the coupled removal mechanisms of the matrix and fibers at various fiber grinding orientations, as well as the effects of grinding speed and maximum undeformed chip thickness (agmax) on material removal behaviors. Results show that fiber properties significantly influence the removal mechanism more than grinding direction. Cracks in fibers propagate perpendicularly to the tungsten core or radially. Increasing grinding speed from 30 m/s to 120 m/s while agmax=0.3 µm reduces matrix smearing and plastic flow traces, while HSG effectively mitigates large-scale fiber fragmentation. When v_s =80 m/s, reducing a_{qmax} from 0.8 µm to 0.1 µm significantly enhances fiber removal quality by transitioning from large-scale fragmentation or fracture to micro-fragmentation, thereby substantially reducing matrix smearing defects on the machined surface.

Keywords:

Metal matrix composites, High-speed grinding, Removal mechanism, Single grain

1 INTRODUCTION

Silicon carbide fiber reinforced TC17 titanium matrix composites (SiCt/TC17) demonstrate significant application potential in aerospace and defense applications due to their high specific strength, rigidity, thermal stability, lightweight nature, as well as superior fatigue and corrosion resistance [Jia et al 2023]. However, due to the inherent brittle-ductile heterogeneity, anisotropy, and large-diameter fiber characteristics (Φ =110 µm), SiCt/TC17 composites are prone to defects such as matrix smearing, fiber fragmentation, and fiber pull-out during conventional machining [Ding et al 2024]. High-speed grinding (HSG) technology offers distinct advantages in reducing wheel wear, improving machining efficiency, and suppressing subsurface damage by enhancing wheel peripheral speeds ($v_s > 45$ m/s) [Zhang et al 2019], providing a viable approach for synergistic removal of SiCt/TC17 matrix and fiber components.

Existing studies confirm the capability of HSG in improving surface integrity of difficult-to-cut materials [Zhang et al 2023]. Li et al. [Li et al 2018, Li et al 2017] systematically

investigated the grinding characteristics of particulate reinforced titanium matrix composites (PTMCs), demonstrating that increased grinding speed effectively reduces grinding forces and surface roughness but increasing grinding temperatures. The material removal mechanism involves coordinated interactions between matrix plastic deformation and reinforcement brittle fracture, where undeformed chip thickness (a_{gmax}) plays a critical role in governing particle removal behavior. Liu et al. [Liu et al 2024] reported that the surface roughness of Inconel 718 alloys exhibits an initial decrease followed by an increase with rising grinding speed, attributed to a dynamic balance between HSG induced suppression of surface smearing and excessive speed triggered brittle fracture. Jiang et al. [Jing et al 2024] identified a "skin effect" in subsurface plastic deformation during Ti6Al4V HSG. showing that when the grinding speed (v_s) was increased from 20 m/s to 220 m/s, the depth of the subsurface plastic deformation layer decreased from 2.8 μm to less than 1 μm .

The single-grain grinding approach simplifies material removal into a three-stage sequence of scratching, plowing, and chip formation, serving as an effective methodology for

analyzing composite removal mechanisms [Liu et al 2025]. Cao et al. [Cao et al 2023] integrated simulation and experimental approaches to reveal multiple failure modes in 2.5D C_f/SiC composites, including edge chipping, fiber breakage, and matrix cracks. Luna et al. [Luna et al 2020] conducted circular path scratch tests to investigate the influence of grain geometry, size, and spacing on the material removal mechanisms of SiC_f/SiC composites. Based on contact mechanics analysis, they concluded that grain shape determines the crack initiation sites, while the fiber orientation governs the crack propagation paths. Yin et al. [Yin et al 2022] observed that edge fragmentation in SiC_f/SiC composites is more pronounced during perpendicular fiber grinding compared to parallel grinding with single grain grinding experiments, and increased grinding speed effectively mitigates edge chipping.

Building upon these foundational studies, the matrix-fiber synergistic removal mechanism in SiCt/TC17 composites was investigated with a single-grain HSG experiment. Through systematic characterization of groove morphology, analysis of brittle-ductile coupled removal behaviors under different fiber orientations, and evaluation of v_s and a_{gmax} effects on material removal mechanisms, this study proposes process optimization strategies for high precision machining.

2 MATERIALS AND METHODS

2.1 Materials

The experimental investigation focuses on SiC_f/TC17 composites fabricated through 1:1 volumetric integration of

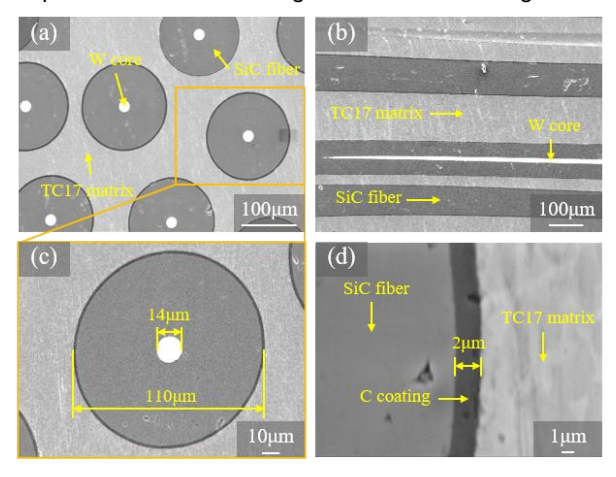


Fig. 1: Micro-structure of SiC_f/TC17 composites

SiC ceramic fibers and TC17 titanium alloy matrix (Ti-5Al-2Sn-2Zr-4Mo-4Cr). Specimen preparation initiates with precise electrical discharge wire cutting of raw materials into 15 mm×10 mm×9 mm standardized blocks, followed by sequential grinding and polishing to achieve requisite surface quality. As illustrated in Fig. 1, the polished surface reveals hexagonal stacking of SiC fibers with average diameter of 110 μm . Each fiber features a 14 μm -diameter tungsten (W) core centrally positioned, encapsulated by a uniform $2\mu m$ -thickness carbon (C) protective coating.

2.2 Grinding setup

The single-grain HSG experiments were conducted on a PROFIMAT MT-408 precision grinding platform (Fig. 2a). Grinding was performed in two directions, along longitudinal fiber (LF) and transverse fiber (TF). Cubic boron nitride (CBN) abrasives (#40/50) were brazed onto stainless steel single-grain core shaft using Cu-Sn-Ti alloy (Fig. 2b, c), then precisely mounted on a Φ400mm wheel via adjustable leveling blocks. Specimen alignment was ensured through dial indicator-assisted calibration in a universal vise, guaranteeing parallelism between machined surface and grinding direction. With constant grinding depth of 20µm, the agmax was controlled through feed rate adjustment while v_s was set to 80m/s, based on established calculation formulae (Equation 1) [Yin et al 2022]. Specifically, when a_{gmax} was set to 0.3 µm, the influence of v_s on machining characteristics was investigated under fixed speed ratios. Detailed experimental parameters are listed in Tab. 1.

$$a_{g \max} = 2\pi d_s \left(\frac{v_w}{v_s}\right) \sqrt{\frac{a_p}{d_s}} \tag{1}$$

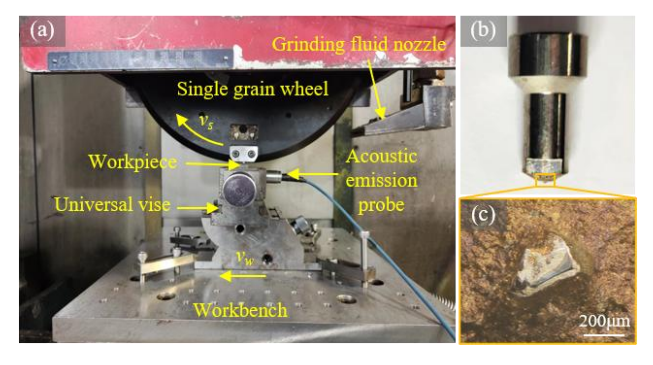


Fig. 2: Experimental setups: (a) grinding platform; (b) single grain core shaft; (c) micro morphology of brazed single CBN grain

Tab. 1: Grinding conditions.

Grinding parameters	Contents	
	Experiments on agmax	Experiments on vs
Undeformed chip thickness a_{gmax} (µm)	0.1,0.2,0.3,0.5,0.8	0.3
Grinding speed v _s (m/s)	80	30,50,80,100,120
Workpiece speed vw (mm/min)	27,54,81,135,216	30,51,81,101,122
Grinding depth a _p (µm)	20	
Grinding fiber orientation	LF, TF	
Diameter of single grain wheel(mm)	400	
Size of grain	40/50#	
Workpiece material	SiC _t /TC17	
Grinding type	Up-grinding	

3 RESULTS AND DISCUSSION

3.1 Grinding along LF

Fig. 3 and Fig. 4 depict material removal characteristics when grinding along LF with varying a_{gmax} and v_s . Groove morphologies exhibit typical damage modes: matrix smearing, matrix burrs, fiber fragmentation, fiber fracture and pull-out, and W-core cut off. Similar to conventional metal matrix composites (MMCs), brittle reinforcement damage dominates surface defect formation. Fiber damage severity escalates with increased a_{gmax} , while v_s shows limited influence on fiber damage patterns.

Under LF, material removal demonstrates stochastic behavior due to continuous fiber-matrix distribution along grinding direction. Considering the 110µm fiber diameter and 200~300µm groove width, individual grinding passes interact with 1-2 randomly distributed fibers. Fiber embedment depth critically determines morphology: decreasing embedment depth induces progressive damage transitions: i) fiber surface microfragmentation (Fig. 3c, Fig. 4b, e); ii) fiber macro fragmentation with W-core cut off (Fig. 3e); iii) fiber macro fracture and pull-out (Fig. 3d, Fig. 4c, e). This aggravation of damage correlates with reduced structural integrity and interfacial bonding strength at shallower embedment depth. Additionally, when fibers are located at the edges of grinding grooves (Fig. 3b, c, Fig. 4b), they tend to experience macro fragmentation or even macro fracture and pull-out.

Comparative analysis of a_{gmax} =0.2 µm (Fig. 3c) versus 0.8µm (Fig. 3f) reveals damage mode transitions from surface micro-fragmentation to macro-fragmentation in deeply embedded fibers. This transition originates from combined compressive-shear stresses exceeding fiber

strength limits, inducing crack initiation and propagation. Increasing agmax intensifies grinding forces: smaller agmax confines cracks to surface layers, whereas larger agmax drives crack penetration and coalescence, culminating in bulk fiber removal. At agmax=0.3 µm (Fig. 3d), non-parallel fiber alignment reduces interfacial strength at shallow embedment regions. The interfacial failure occurs under the shear stress, while stress concentration induced by their compressive force leads to median cracks propagating through the fiber cross-section, ultimately resulting in fiber macro fracture and pull-out cavity defects. For $a_{qmax} = 0.5$ μm (Fig. 3e), energy release from median cracks surpasses W-core fracture energy, causing complete W-core rupture and subsequent fiber macro-fragmentation. Matrix removal couples strongly with fiber damage: fiber macrofragmentation or pull-out creates height differentials that induce lateral matrix flow and burr formation. Continuous matrix distribution along grinding direction promotes elongated burrs at groove edges (Fig. 3b, c).

Experimental results demonstrate limited effects on fiber damage modes: v_s from 30m/s (Fig.4b) to 100m/s (Fig.4e), deeply embedded fibers exhibit only surface microfragmentation. Additionally, distinct matrix covering is observed on fiber surfaces at v_s =100 m/s, which results from severe work hardening in the surface titanium alloy layer caused by combined effects of insufficient heat dissipation from the grinding zone under HSG and the inherently low thermal conductivity of titanium alloys. At v_s =50 m/s (Fig.4c), shallowly embedded fibers experience combined interfacial debonding and macro-fracture, evidenced by large fracture debris. At vs=100 m/s, plastic deformation features at W-core fracture surfaces become evident, confirming direct grain-W-core contact during machining process.

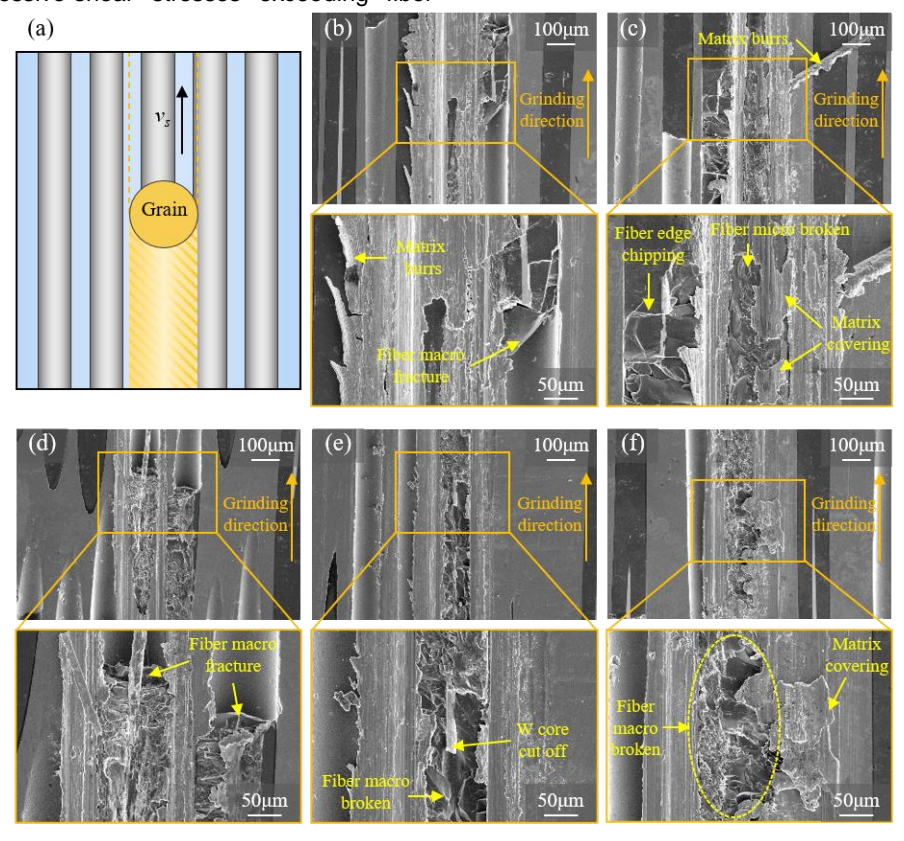


Fig. 3: Grinding grooves morphology of SiCt/TC17 when grinding along LF and ν_s=80 m/s. (a) schematic diagram of single-grain grinding; set a_{gmax}: (b) 0.1 μm (c) 0.2 μm (d) 0.3 μm (e) 0.5 μm (f) 0.8 μm.

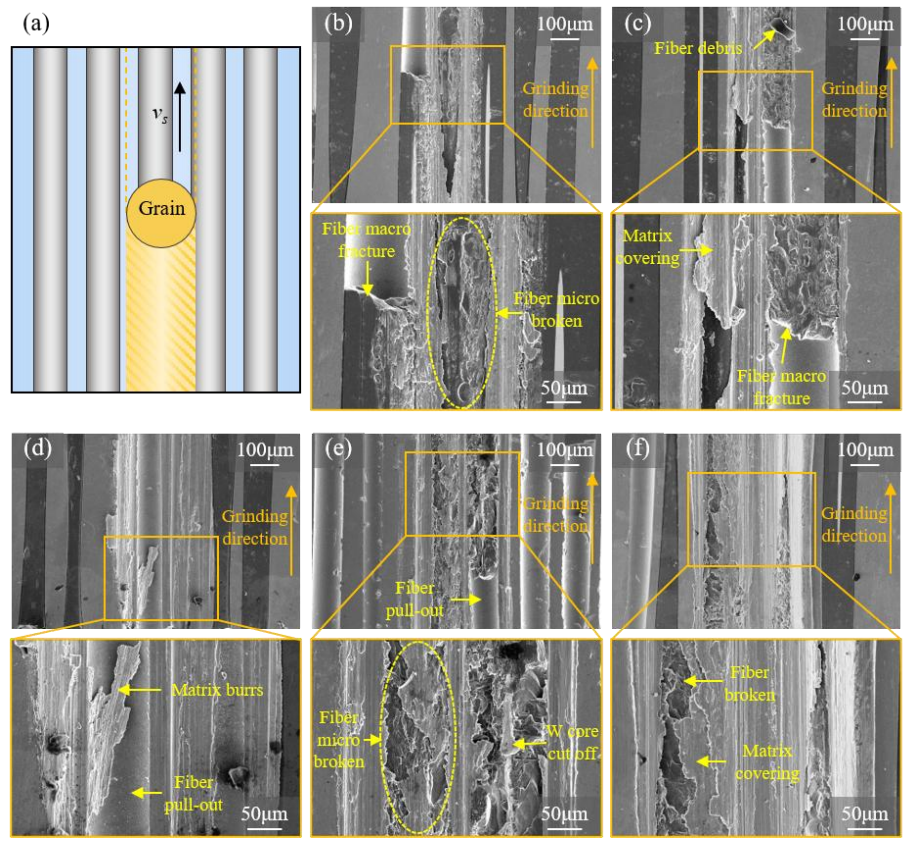


Fig. 4: Grinding grooves morphology of SiC_t/TC17 when grinding along LF and a_{gmax}=0.3 μm: (a) schematic diagram of single-grain grinding; set v_s: (b) 30 m/s (c) 50 m/s (d) 80 m/s (e) 100 m/s (f) 120 m/s.

Under these conditions, the combined effects of compromised fiber integrity and active W-core participation in material removal significantly enhance radial crack propagation depth within fibers, resulting in fiber macrofragmentation. The brittle fracture or pull-out of fibers along the grinding groove base creates step-like height differentials between fiber and matrix phases perpendicular to the grinding direction, thereby inducing stress-driven lateral plastic flow in the matrix material (Figs. 4d, f).

3.2 Grinding along TF

Fig. 5 and Fig. 6 illustrate the material removal morphology of SiC_t/TC17 composites when grinding along TF under varying a_{gmax} and v_s . Under TF, The grinding groove characteristics primarily include: matrix covering, fiber fragmentation, fiber macro fracture and pull-out, and W core exposure/deformation/cut off. Grinding along TF engages a greater number of fibers in the grinding process compared to LF, with reinforced fiber damage constituting the dominant surface defects. Fiber embedment depth critically determines removal morphology evolution, demonstrating progressive damage intensification with increasing a_{gmax} while maintaining negligible sensitivity to v_s variations.

Unlike ceramic matrix composites (CMCs) where brittle matrix shattering predominates, the ductile titanium matrix in SiCt/TC17 absorbs mechanical energy through elastoplastic deformation, effectively mitigating stress concentration and reducing fiber removal damage. Consistent with observations under LF, decreasing fiber embedment depth under TF induces multiple removal mechanisms: i) fiber surface micro fragmentation (Fig. 5b, d); ii) fiber fragmentation with W-core exposure (Fig. 5c, f, Fig. 6b, d, f), W-core deformation (Fig. 5b, d, e, Fig. 6e); W-core cut off (Fig. 5c, d, Fig. 6c); iii) fiber macro-fracture and pull-out (Fig. 5e, Fig. 6b, c). The reduction in fiber

embedment depth compromises structural integrity, leading to a progressive increase in fiber removal damage. Mechanistically, the W-core within the fiber structure induces preferential crack propagation along the W-SiC interface characterized by low fracture energy. This interfacial failure mechanism results in the preferential fracture and detachment of the SiC matrix encapsulating the W-core. Furthermore, the weakly bonded interface design exacerbates interfacial strength degradation with embedment depth reducing. This synergistic effect facilitates interface delamination and fiber macro-fracture, ultimately inducing fiber pull-out cavity under grain action.

When a_{gmax} increased from 0.2 µm (Fig. 5c) to 0.5 µm (Fig. 5e), similarly observed fiber fragmentation accompanied by W-core exposure was present. However, the fiber fragmentation near the W-core becomes more pronounced at larger a_{gmax} , resulting in evident cavity defects formation. Compared with LF, the alternating fiber-matrix distribution characteristic of TF effectively suppresses continuous burr formation. The increase in a_{gmax} not only enhances chip removal in the metallic matrix but also intensifies fiber removal-induced damage, leading to a severe matrix covering fiber surfaces phenomenon (Fig. 5f).

When the grinding speed increased from 30 m/s (Fig. 6) to 80 m/s (Fig. 6d) and 120 m/s (Fig. 6f), fiber surface fragmentation accompanied by W-core exposure was consistently observed, indicating similar fiber embedding depths. Notably, the grinding speed appeared to exert no significant effect on the brittle removal mechanism of fibers. Meanwhile, the TC17 matrix removal pattern at the grinding groove bottom transitioned from pronounced grinding scratches to smoother surfaces with $\nu_{\rm S}$ increasing. Furthermore, analogous to LF, insufficient heat dissipation in the grinding zone during high-speed processing along TF

MM SCIENCE JOURNAL I 2025 I Special Issue on HSM2025

resulted in more distinct work hardening on matrix surfaces and severe matrix covering on fiber surfaces.

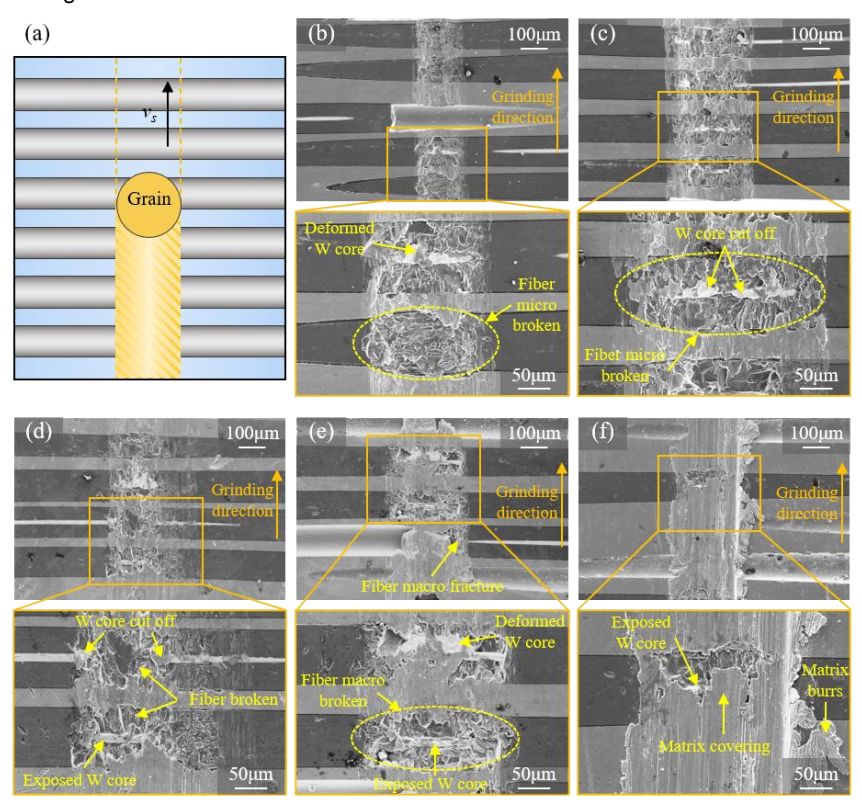


Fig. 5: Grinding grooves morphology of SiC_t/TC17 when grinding along TF and v_s =80 m/s: (a) schematic diagram of single-grain grinding; set a_{gmax} : (b) 0.1 μ m (c) 0.2 μ m (d) 0.3 μ m (e) 0.5 μ m (f) 0.8 μ m.

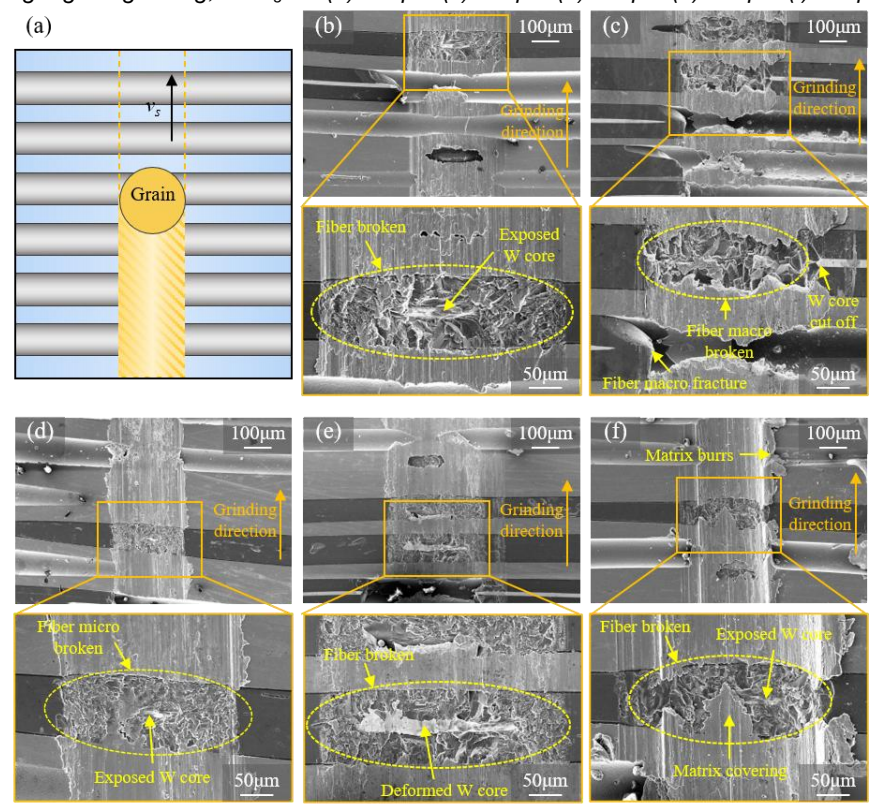


Fig. 6: Grinding grooves morphology of SiC_t/TC17 when grinding along LF and a_{gmax}=0.3µm: (a) schematic diagram of single-grain grinding; set v_s: (b) 30 m/s (c) 50 m/s (d) 80 m/s (e) 100 m/s (f) 120 m/s.

4 CONCLUSIONS

This study conducted HSG on SiC_t/TC17 composites with single CBN grain. The influences of fiber orientation, a_{gmax} and v_s on the material removal mechanisms were investigated. The specific conclusions are as follows:

- (1) The removal mechanisms of LF involve matrix covering, matrix lateral plastic flow, fiber surface microfragmentation, fiber macro fragmentation, fiber macrofracture and pull-out, fiber edge chipping, and W-core cut off. The dominant removal mechanisms of TF include matrix covering, fiber surface microfragmentation, fiber fragmentation, fiber macropull-out. fracture and and W-core exposure/deformation/cut off. Under LF, fiber macrofracture and pull-out phenomena were more matrix covering pronounced, whereas the phenomenon became predominant under TF.
- (2) Consistent with traditional MMCs, the removal damage of reinforcement dominates surface defect formation. Fiber embedment depth critically governs damage evolution in both orientations: Reduced of embedment depth diminishes fiber structural integrity and interfacial strength, driving transition of fiber removal model from micro-fragmentation to macro-fracture.
- (3) Under both fiber orientations, a_{gmax} exerted significant influence on fiber removal damage. With a_{gmax} increasing, the crack propagation depth within fibers exhibited marked augmentation, resulting in fiber macro-fragmentation and distinct cavity defects. Concurrently, matrix covering intensify proportionally to a_{gmax} , which was attributed to dual mechanisms: enhanced chip removal of ductile metal matrix and amplified fiber damage-induced height differential along the grinding direction between fibers and matrix. While increasing v_s demonstrated negligible effects on fiber removal damage, but effectively suppressed matrix scrathes at grinding groove bottoms.

5 REFERENCE

[Jia 2023] Jia, Q. Y., Wang, Y. M., Zhang, X., et al. Multiscale failure mechanism analysis of SiC fiber-reinforced TC17 composite subjected to transverse tensile loading at elevated temperature. Acta Metallurgica Sinica-English Letters, 2023, 36: Vol.36, No.6., pp 1007–1022. ISSN 1006-7191.

[Ding 2024] Ding, W. F., Liu, G. Q., Chen, T., et al. Effects of fiber orientations on removal behaviors in ultrasonic vibration-assisted grinding continuous fiber reinforced Ti matrix composite. The International Journal of Advanced Manufacturing Technology, 2024, Vol.133, pp 4223–4234. ISSN 0268-3768.

[Zhang 2019] Zhang, B., Yin, J. F. The "skin effect" of subsurface damage distribution in materials subjected to high-speed machining. International Journal of Extreme Manufacturing, 2019, Vol.1, No.1., pp 022003. ISSN 2631-8644.

[Zhang 2023] Zhang, J., Shang, X., He, B., et al. Towards understanding the crack suppression mechanism in brittle materials with high grinding speed at different temperatures. International Journal of Machine Tools and Manufacture, 2023, Vol.193, pp 104088. ISSN 0890-6955. [Li 2018] Li, Z., Ding, W. F., Liu, C. J., et al. Grinding performance of TiC_p/Ti-6Al-4V composites with CBN wheels, part I: experimental investigation and surface

features. Procedia CIRP, 2018, Vol.77, pp 525–528. ISSN 2212-8271.

[Li 2017] Li, Z., Ding, W. F., Liu, C. J., et al. Prediction of grinding temperature of PTMCs based on the varied coefficients of friction in conventional-speed and high-speed surface grinding. The International Journal of Advanced Manufacturing Technology, 2017, Vol.90, No.5-8., pp 2335–2344. ISSN 0268-3768.

[Liu 2024] Liu, H., Han, H., Jiang, Q., et al. Mechanisms in the machinability improvement of Inconel 718 superalloy through ultra-high-speed grinding. Journal of Materials Processing Technology, 2024, Vol.333, pp 118614. ISSN 0924-0136.

[Jiang 2024] Jiang, Q., Li, S., Liu, H., et al. Material removal mechanisms in ultra-high-speed scratching of Ti6Al4V alloy by selective laser melting. Journal of Manufacturing Processes, 2024, Vol.127, pp 645–659. ISSN 1526-6125. [Liu 2025] Liu, Y., Wang, Y. Z., Zhao, Z. G., et al. Investigation on 2D SiCt/SiC composite scribing mechanism by single- and double-grit. Composite Structures, 2025, Vol.351, pp 118547. ISSN 0263-8223. [Cao 2023] Cao, C., Song, Q. H., Fu, H., et al. Fiber orientation effects on grinding characteristics and removal mechanism of 2.5D Ct/SiC composites. Chinese Journal of Aeronautics, 2023, Vol.36, No.12., pp 425–441. ISSN 1000-9361.

[Luna 2020] Luna, G. G., Axinte, D., Novovic, D., et al. Influence of grit geometry and fibre orientation on the abrasive material removal mechanisms of SiC/SiC Ceramic Matrix Composites (CMCs). International Journal of Machine Tools and Manufacture, 2020, Vol.157, pp 103580. ISSN 0890-6955.

[Yin 2022] Yin, J. F., Li, M., Xu, J. H., et al. Edge chipping characteristics in grinding SiC_f/SiC composite. Ceramics International, 2022, Vol.48, No.5. pp 7126–7135. ISSN 0272-8842.